Full Length Article

Structural design and analysis of a servo crank press

Recep Halicioglu [a,*], Lale Canan Dulger [b], Ali Tolga Bozdana [b]

[a] Osmaniye Korkut Ata University, Mechanical Engineering Department, 80000 Osmaniye, Turkey
[b] Gaziantep University, Mechanical Engineering Department, 27000 Gaziantep, Turkey

ARTICLE INFO

ABSTRACT

Due to precision, flexibility, simplicity in construction, easy control, higher speed and lower energy consumptions, servo presses have recently become popular in metal forming applications. Servo press technology combines the advantages of hydraulic and conventional mechanical presses without their drawbacks. This study presents design, construction and demonstration of a servo crank press system for metal forming operations. The research involves structural design and analysis with dynamic considerations of the servo press. A design and manufacturing guide is offered. The press used in this work has a load capacity of 500 kN and stroke capacity of 200 mm. Structural CAD model is constructed, and Finite Element Analysis (FEA) of press parts are performed within safety limits. Experimental studies are performed on this machine. Satisfaction at the output is seen.

1. Introduction

Design is either formulation of a plan for needs or a solution for a problem, in which some parameters are desired like functionality, safety, reliability, manufacturability, and marketing consideration. A design must have some processes such as identification of need, definition of problem, synthesis, analysis, optimization, evaluation and presentation. Design can involve more than one discipline of mechanical engineering such as dynamics, fluid mechanics, heat transfer and manufacturing technology [1–3]. The structural design in mechanical analysis can be applied by Finite Element Method (FEM), which is a numerical technique for finding approximate solutions to boundary value problems for differential equations. FEM allows detailed visualization of where the structures bend or twist, and indicates the distribution of stresses and displacements [4].

Several studies on structural design and analysis of machine parts and tools are found in the literature [5–11]. FEM simulations are performed by using Ansys® software [12,13] although other software firms have started to provide dedicated analysis packages (e.g. SolidWorks®) in recent years. SolidWorks® allows 3D CAD, FEA, motion analysis, and simulation modules. Some studies on use of SolidWorks® are also reported in design and analysis

[14–18]. Crank presses are assembly of slider crank mechanisms [19]. The following studies involve crank press or slider crank design, manufacturing, and FEA. Doege [20] designed a crank press with a noncircular gear for deep drawing stroke motion. The study showed mechanical modernizations for the desired motion of press by changing gears. Spiewak et al. [21] studied on predictive monitoring and control of the cold extrusion process. A crank press and its mechanisms were defined under high loading at high speeds. They developed a multicomputer system to present the results showing feasibility of predictive monitoring, diagnosis and control.

Chang and Joo [22] presented a study to support design optimization of engineering products, including High Mobility Multipurpose Wheeled Vehicle (HMMWV). In proposed environment, Pro/engineer® and SolidWorks® were employed for product model representation, Dynamic Analysis and Design System (DADS) was employed for dynamic simulation of mechanical systems including ground vehicles, and Design Optimization Tool (DOT) was included for a batch mode design optimization. In their research, the overall finite difference method was adopted to support design sensitivity analysis. A simple slider-crank mechanism and HMMWV were optimized to demonstrate feasibility and effectiveness of the proposed system. Having applied optimization is rod length/crank length ratio is found 5. Abdullah and Telegin [23] studied dynamic analysis of a hot-crank press. Definition of the slider-crank mechanism (size, mass, inertia, etc.) and deformation analyses were given for each mechanism part. Zheng and Zhou [24] described a flexible coupling model of the slider-crank mechanism because of

* Corresponding author.
  E-mail addresses: rhalicioglu@osmaniye.edu.tr, recephalicioglu@gmail.com (R. Halicioglu).

Peer review under responsibility of Karabuk University.

its accuracy by using Adams®. The dynamic simulation results of mechanism with clearance under no-load and piling conditions were presented.

Servo presses driven by servo motors have recently come into prominence for sheet metal forming operations due to their flexibility, controllability, and simplicity. Kutuk and Dulger [25] studied on motion design of a hybrid servo press. The press has two cranks are driven by one servo motor and one constant velocity motor. Halicioglu [26] has then presented a complete study on design, synthesis, manufacturing and control of servo crank press.

A design guide involving system dynamics, load types, and capacities are defined. Pre-strength analysis is put into rule, which should be specified and applied. In this study, the design guide of a servo crank press is prepared, and its structural 3D CAD model is constructed. FEA of all parts are investigated using SolidWorks®. Manufactured press is presented herein.

2. Description of the servo press and design methodology

A servo crank press mechanism is similar to conventional crank press mechanism without flywheel and clutch-brake. Its parts are servo motor with controller panels, mechanisms (crank-connecting rod-ram), gears (pinion and main gears), bearings, and structural body (as C frame and mono-block). Sketch of the model is given in Fig. 1. It includes body and mechanism, in which the crank length, the crank angle, the rod length, the rod angle, and the slider (ram) position are represented by r, θ, l, β, and y, respectively. TDC and BDC refer to Top Dead Center and Bottom Dead Center. The rod-to-crank ratio is taken as 7 [26]. Dimensional specifications of press are given in Table 1. Table 2 presents choice of materials for the parts of press machine referred to Coskunoz Metal Form [27].

A design approach is considered as design guide is given in Fig. 2. The requirements are given by press users by specifying dynamic expectations. Having performed the dynamic analysis, loads and motion parameters are used for the machine parts; dynamic and static. The machine parts are designed in accordance

Table 1
Press specifications.

In CE standards C type crank press	
Load capacity	500 kN
Stroke	200 mm
Stroke-ram adjust	150 mm
Ram (in TDC)-bolster distance	500 mm
Bolster plate size	800×500 mm^2

Table 2
Chosen materials for the press parts.

Tool part	Material	Yield strength (MPa)	Tensile strength (MPa)
Ram	St52	360	530
Connecting rod	St52	360	530
Crankshaft	42CrMo4	750	1000
Pinion shaft	42CrMo4	750	1000
Main body	St37	275	370
Bolster plate	St37	275	370
Main gear	GS52	360	530
Pinion gear	30CrNiMo8	1050	1250

with a satisfactory engineering design that is necessary for 3D CAD design. The steps on machine parts are analyzed by FEM.

The previous studies present kinematic and dynamic analysis of crank press mechanism [26,28,29]. This study includes some dynamic parameters that are found based on information given in the previous studies. Press motion and dynamic loading were represented in the previous studies. The motion profile is defined based on ram. The most preferred scenarios are chosen for its operation. It is considered that the rated force on slider is applied less than 7 mm stroke position for mechanical structure design.

3. Bearing design

The press mechanism's joints are created by using hydrodynamic sleeve bearings, roller bearings, and slide ways. Roller
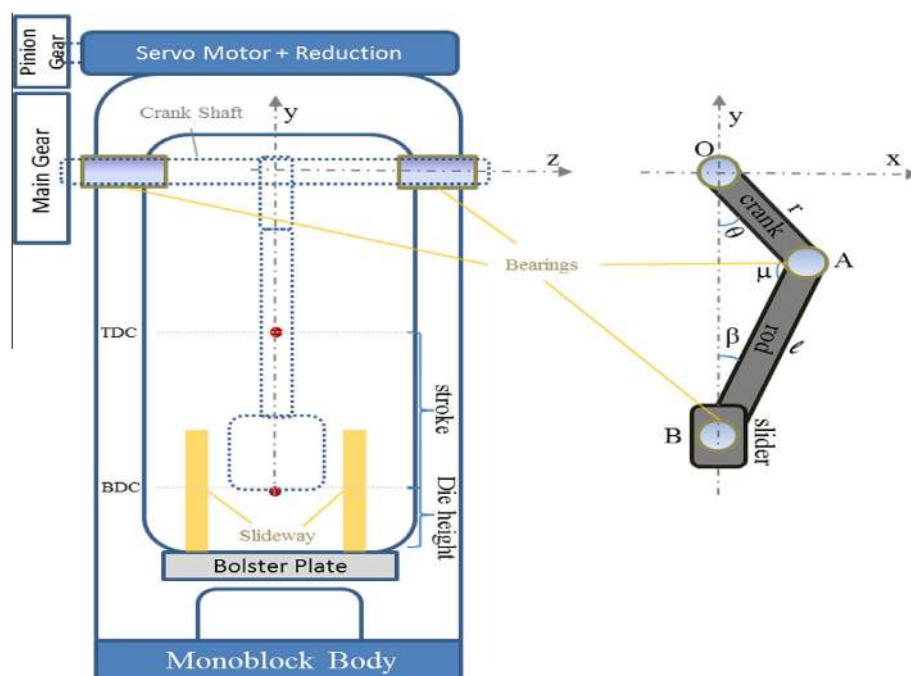

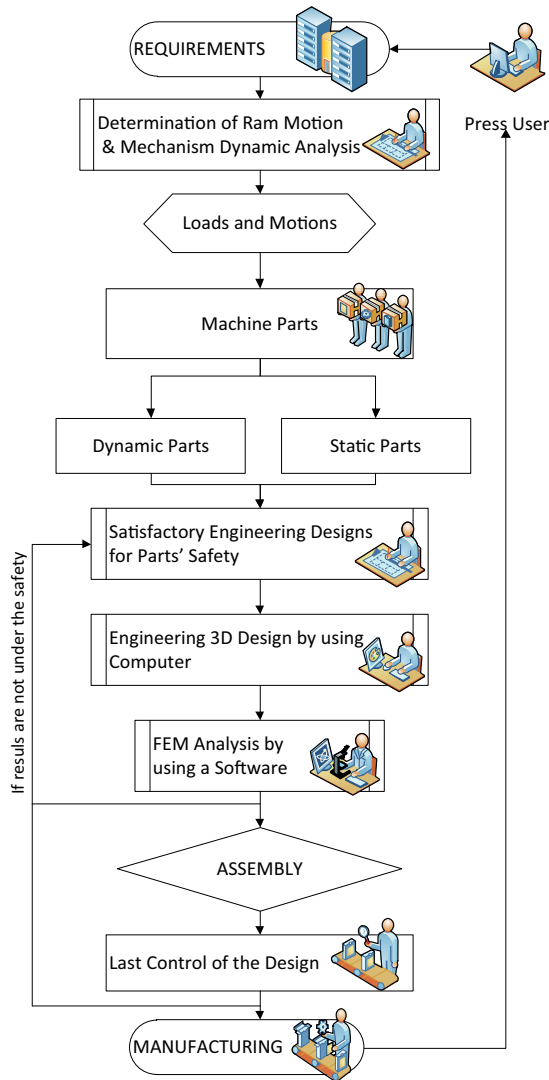**Fig. 1.** Sketch of the press structure.

Fig. 2. Design and manufacturing guide (the press machine).

bearings are generally used for low loaded contacts. They are used between the main body and the pinion shaft without radial forces. Sleeve bearings can be used under high radial forces by lubrication systems. While main body and crank, crank and connecting rod, connecting rod and ram are connected together by sleeve bearings, ram and main body are connected together by sideways. As all of the joints are under high loads in the press mechanisms with low velocities. The most useful material for a bearing is bronze alloy since they have superior boundary lubrication characteristics [1,3,30–32].

3.1. Bearing design considerations

Bearing design is based on the capacity of material's nominal bearing stress (*P*) as formulated in Eq. (1) [33] where *F*, *B* and *D* are nominal force, bearing width, and bearing diameter, respectively. The maximum load and speed limit as well as lubricated wear must be under the critical values. Diametric wear and energy loss equations are given through Eqs. (2) and (3) where d, V, E_{loss}, K, t_s, H, f are diametric wear, speed, energy loss, wear coefficient, total sliding time, hardness, and friction coefficient, respectively. Eq. (4) depends on energy loss indicating to bearing temperatures. T_b, T_a, h_a, A_b are representing bearing temperature, ambient temperature,

ambient heat transfer coefficient, outer surface area of bearing house, respectively.

$$P = \frac{F}{BD} \tag{1}$$

$$d = K\frac{PVt_S}{H} \tag{2}$$

$$E_{loss} = fFV \tag{3}$$

$$T_b = T_a + \frac{E_{loss}}{h_a A_b} \tag{4}$$

According to Eqs. (2) and (3), diametric wear and energy loss depend on *PV* factor. Their values are obtained experimentally on material catalogues. Tin bronzes are selected because of their higher bearing stress, less diametric wear and relative cheapness [1,3,30–32,34]. Besides, determination of *B*/*D* ratio can be taken. Eq. (5) can be used for spherical plate bearings. *K* is the spherical diameter and *C* is the outer ring width [35].

$$P = \frac{F}{KC} \tag{5}$$

Some assumptions are taken in this study. The forces, *F* (N) is constant and taken as maximum value. The area, *A* (mm²) is variable by *B*/*D* ratio. The angular velocity, *W* (rad/s) is constant and taken as its maximum values. The bearing dimensions, i.e. *B* (mm) and *D* (mm), and the bearing *PV* factors.

3.2. Bearing design procedure

The crank press consists of four parts: crank, connecting rod, ram, and main body. All parts are assembled to each other with bearings. The mechanism and their contact faces (*CFs*) are represented in Fig. 3. The cylindrical bearing material is selected as tin bronze (ASTM B505) for high-load sleeve bearings [10]. The material for other bearings are high hardenability antifriction bearing steel (ASTM A485).

There are two bearings on the connecting rod; radial journal bearing and spherical plate sleeve bearing. There are two radial journal bearings on the crankshaft. There are two slider bearings on the main body for sliding ram. There is friction between active bearings and sleeve parts. The bearing material of ASTM B505; P_{max} = 35 MPa, V_{max} = 1.3 m/s. It is desired that maximum PV < 4 MPa*m/s [36,37]. For spherical and linear plate bearing,

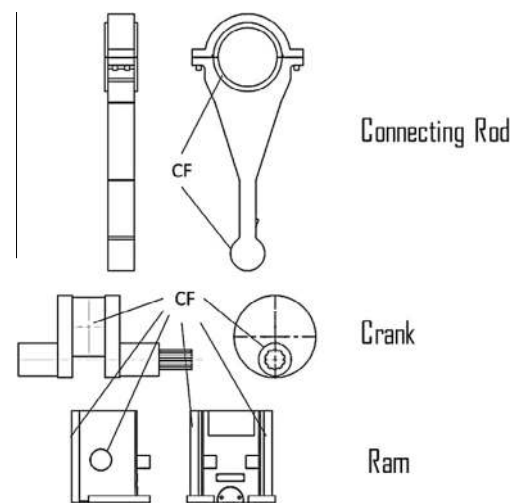**Fig. 3.** Contact Faces (CFs).

Table 3
Bearing characteristics (Crank-Press).

Bearings (between)	Velocity[a] (m/s)	Force (kN)	D (mm)	B (mm)	c (mm)	t (mm)
Crank–Connecting rod	2	500	200	130	0.055	12–19
Connecting rod–Ram	0.25	500	95	Spherical	0.015	–
Crankshaft–Main body	2	250	95	150	0.022	8–11
Slide ways	0.15	15	35 (width)	500	–	–

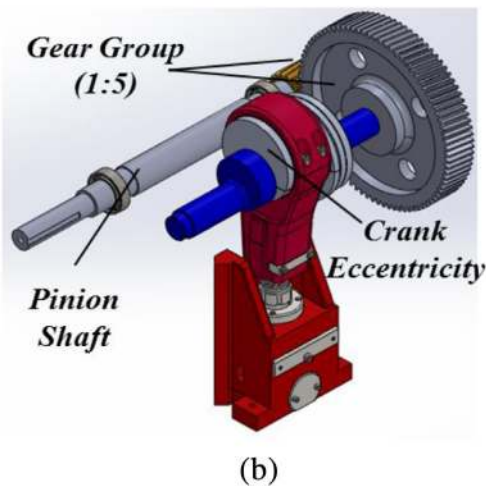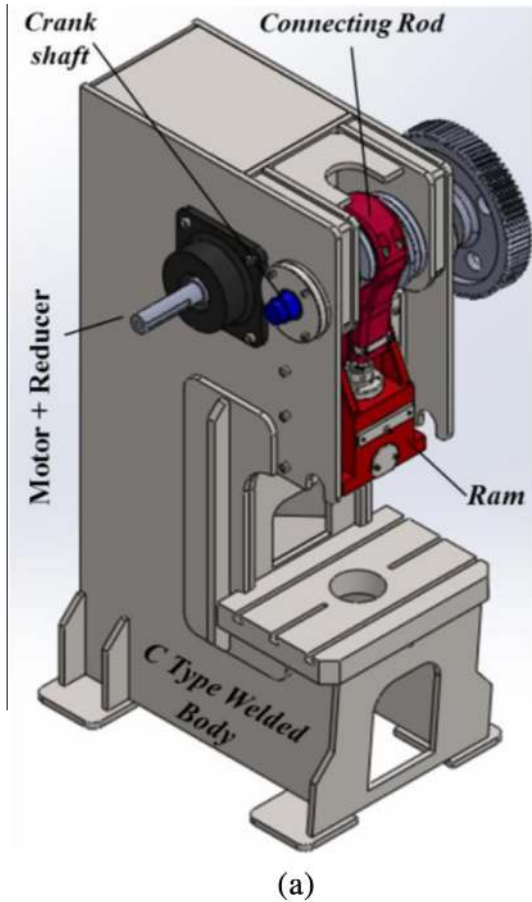[a] Velocities are considered under maximum force.

Fig. 4. Solid model of the press: (a) complete assembly, (b) transmission mechanism.

the material is ASTM A485 with static contact pressure capacity of 430 MPa and *PV* limit of 2.8 MPa*m/s (without oil lubrication) [35]. The steps for design of bearing are presented in Appendix A1. Bear-
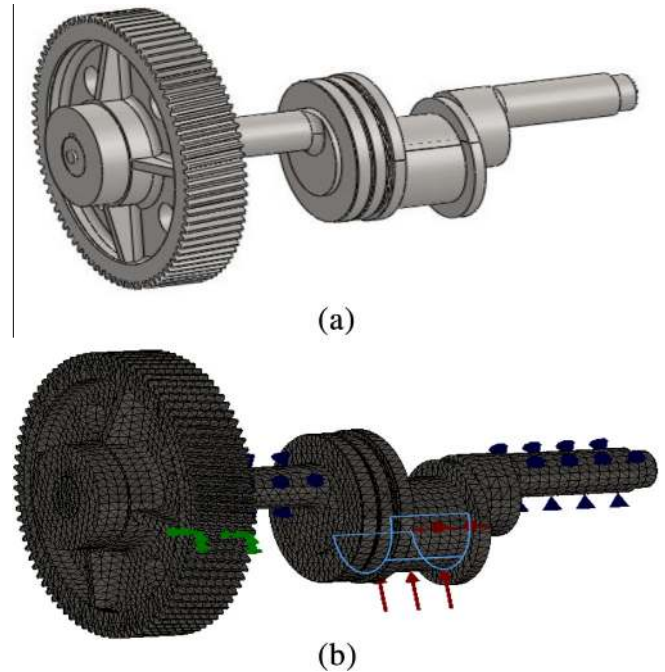

Fig. 5. (a) Solid CAD model of the crank assembly, (b) Loading and boundary conditions on meshed model of the crank assembly.

ings crank–connecting rod, crankshaft–main body, and connecting rod–ram are determined by the maximum velocity and the force from the dynamic analysis, Table 3.

4. Structural design

Strength and size of press mechanisms and main body is determined before 3D CAD design and assembly of each part. The calculations are performed static since the loading of press starts near BDC. Five parts of the press are designed according to their safety conditions. Strength calculations and determination of the critical part dimensions are specified for connecting rod design, crankshaft design, ram design, gear design (with keyways), and main body. According to forming press application, SF is selected by classical rule of thumb Eq. (6) as $2 \leqslant$ SF [38]. For the overall system; material properties are selected by manufacturer's values ($SF_{material} = 1.1$), loads are well defined as static ($SF_{stress} = 1.1$), dimensions are adjusted on average manufacturing tolerances ($SF_{geometry} = 1.0$), failure analysis is not well developed ($SF_{failure} = 1.3$), and reliability must be high ($SF_{reliability} = 1.3$). Yield stresses are used in calculation of SF in Eq. (7) [39]. While the principle strength is yield strength (σ_y), shear strength (τ_y) is considered as 0.58 σ_y for steel and its alloys and 0.75 σ_y for iron [36].

$$SF = SF_{material} \times SF_{stress} \times SF_{geometry} \times SF_{failure} \times SF_{reliability} \qquad (6)$$

$$SF = \frac{Yield\ strength}{Allowable\ design\ stress} \qquad (7)$$

Table 4
Crank simulation details.

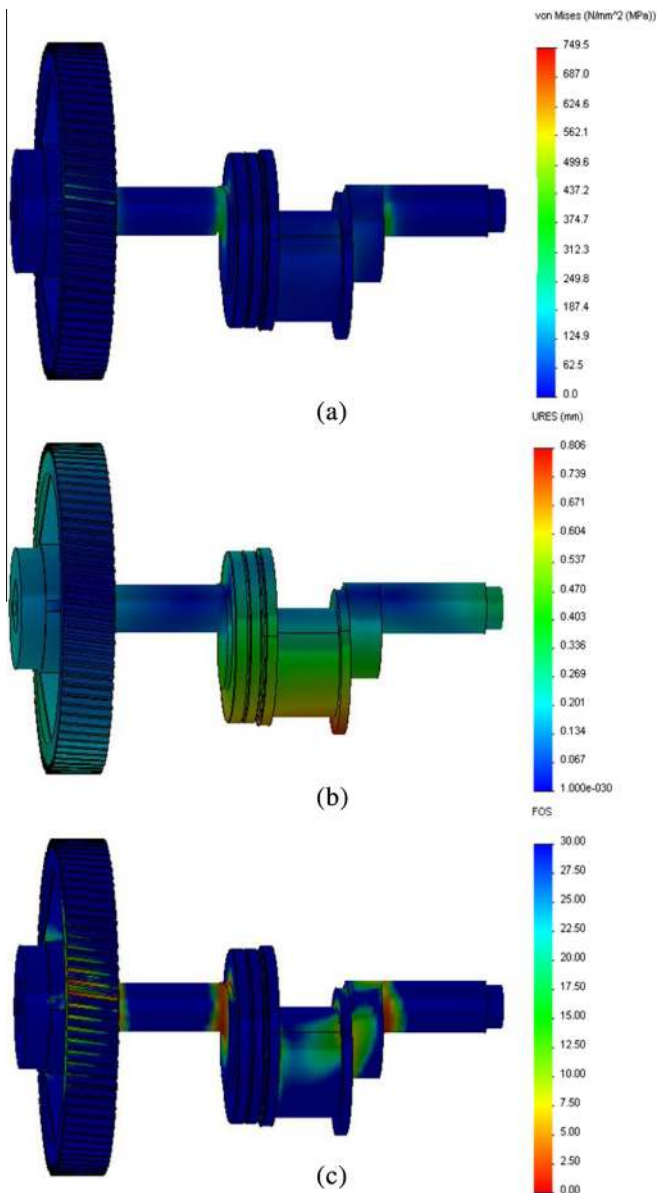| Crank material: 42CrMo4	Main gear material: GS52
Mesh	
Number of nodes: 128,300	Number of elements: 81,515
Global size: 17 mm	Tolerances: 0.85 mm
FEA	
von Mises stress: 749.5 MPa	Max. deformation: 0.806 mm

Fig. 6. Structural analysis results of the crank assembly: (a) von-Mises stress, (b) Deformation, (c) Factor of safety.

There are five parts on servo crank press: main body, crank, connecting rod, ram, and pinion shaft. These parts are designed according to the bearing dimensions. There are two gears and three keys. One of them is on the crankshaft between crankshaft and main gear. The others are on the pinion shaft between pinion gear-pinion shaft and pinion shaft-gear box. The maximum torque of 20,000 Nm is considered for the crankshaft and gear ratio of 1:5 is selected between pinion and crankshaft. Maximum torque of 4000 Nm is applied on the pinion shaft. The maximum power for system is 25 kW. Two helical gears (module: 7, angle: 5°) and three connecting keys are designed [2,30,40].

The 3D CAD model of the press was built using SolidWorks® where the mass-inertias were found by the software [41]. Fig. 4 (a)-(b) show 3D solid model of the system with the mechanism.

5. Finite element analysis

The strength is important for the servo press as it is treated as a heavy duty machine tool. If strengths of parts are under the desired values, the design must be started again. Critical parts are assembled and their FEA is completed by using SolidWorks® Simulation Toolbox [41]. Initially meshes of each part are created according to the structure. Force and boundary scenarios are determined on each part with FEM simulations.

5.1. Assembly of crank

Assembly of crank is constructed by crankshaft, the eccentricity group, and the main gear in Fig. 5. It was assumed that crank assembly is considered as mono block, and one gear contact surface (1720 mm²) is fixed. Main gear is mounted on crankshaft with a key and interference fit. Fig. 5 shows the meshed model of the crank group. Discretization (mesh generation) is performed. The component is divided into a number of small parts. Table 4 shows details during mesh procedure. The mesh is high quality due to the fact that the effect of force on each portion of the component is not the same. Crankshaft has a constraint with journal bearings: from two sides of bearings those are press fit to crankshaft with 60,580 mm² surface area. Only 180° of the bearing surfaces facing the load direction is the constraint for motion of crankshaft. This constraint is defined as a fixed semicircular surface that is as wide as journal bearing width. The distribution of load over connecting rod bearing causes uniform pressure along 157° of contact area. Since crankshaft is in interaction with connecting rod, the same loading distribution is transmitted to the crankshaft. The force which is 500 kN in total is considered as a pressure of 18.8 MPa applied on the crank eccentricity contact area (41,250 mm²) near BDC position of the ram. Fig. 6 shows the results of analyses based on loading conditions with boundary conditions. Navy blue arrows indicate bearings (surface area: 59,360 mm²), green arrows indicate the fixed surfaces, and red arrows indicate applied pressure on the crank assembly. The total deformation and von-Misses
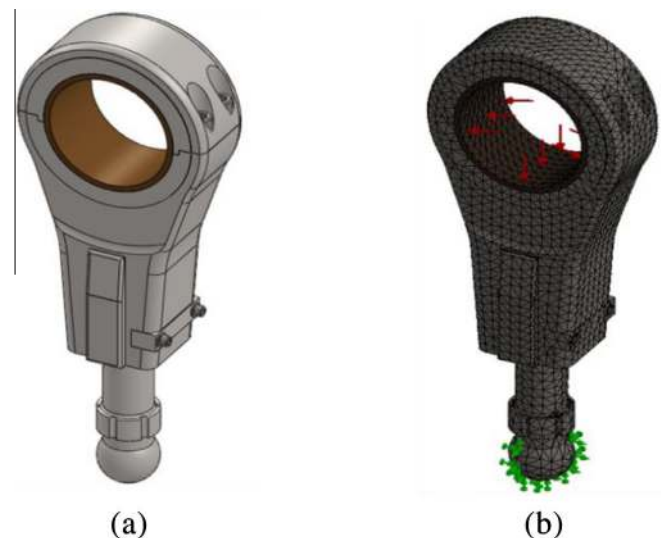

Fig. 7. Connecting rod assembly: (a) Solid CAD model, (b) Meshed model with loads and fixtures.

Table 5
Connecting rod simulation details.

Connecting rod material: St 52	
Mesh	
Number of nodes: 45,820	Number of elements: 27,843
Global size: 17 mm	Tolerances: 0.85 mm
FEA	
Max. von Mises stress: 244.4 MPa	Max. deformation: 0.559 mm

stresses acting on the crankshaft are found. When the force is applied, a slight deformation with low stresses take place in the crank assembly. The stresses acting on crankshaft are shown in Fig. 6(a). The maximum stresses acting on the crank assembly are indicated by red color. The deformation of crankshaft is presented in Fig. 6(b), and Fig. 6(c) shows the values for factor of safety (SF is indicated as FOS in simulation). Table 4 also shows details of FEA. The minimum safety of the shaft is about one. This value is not the actual value. There are corners on the shaft, which are very small sections. In fact, SF is over 3 for the entire crank assembly system.

5.2. Connecting rod assembly

Assembly of connecting rod is constructed by bottom part, top part, bearing, and screw (with knob) in Fig. 7(a). There are certain assumptions that connecting rod assembly is considered as mono block, and contact surface (23,300 mm^2) for knob is fixed. Connect-

ing rod length is taken as 700 mm. Mesh details are given in Table 5. Fig. 7(b) shows the meshed model of connecting rod group. Connecting rod is in interaction with crankshaft, and hence the same loading distribution is transmitted to the crankshaft. In this study, the force which is 500 kN in total is considered as a pressure of 18.8 MPa applied on the crank eccentricity near BDC position of the ram. A fixed reaction surface is considered on the knob. Fig. 7(b) shows loading and boundary conditions (contact surface area: 41,250 mm^2). Green arrows indicate fixed surfaces while red arrows indicate applied pressure on the connecting rod assembly. After the boundary conditions and forces are applied, structural analysis of the connecting rod assembly is performed. The main concern is the total deformation and von-Mises stresses acting on the connecting rod assembly.

The stresses are shown in Fig. 8(a) where the maximum stresses are indicated by red color. The total deformation is shown in Fig. 8(b). The portions in red and blue colors show that the deformation at those regions is the maximum and the minimum, respectively. Fig. 8(c) presents the values for SF. Table 5 also shows results of FEA. While the minimum safety of the shaft is about 1.5 on the bearing, this value is actually over 3 for the entire assembly.

5.3. Ram assembly

Assembly of ram is constructed by safety block, spherical bearing, and main body as given in Fig. 9(a). Table 6 shows ram mesh
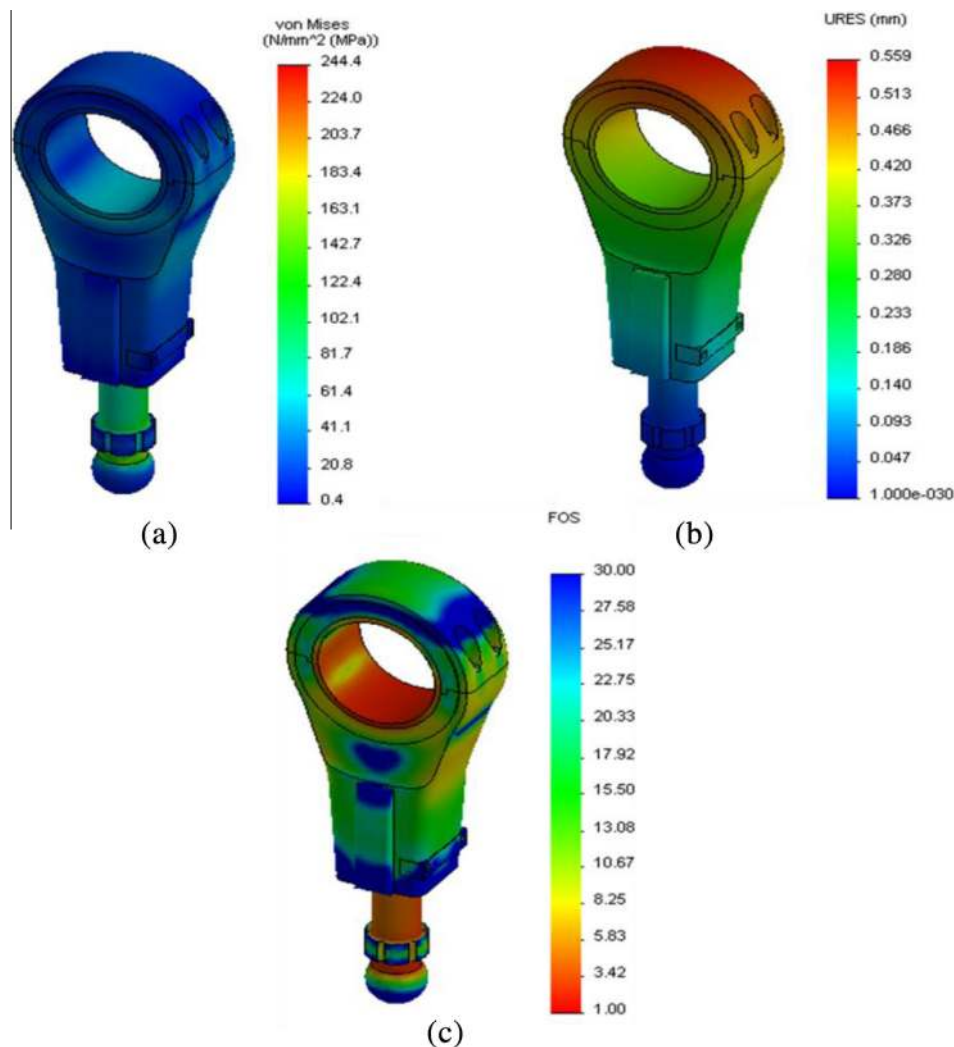

Fig. 8. Structural analysis results of the connecting rod assembly: (a) von-Mises stress, (b) Deformation, (c) Factor of safety.
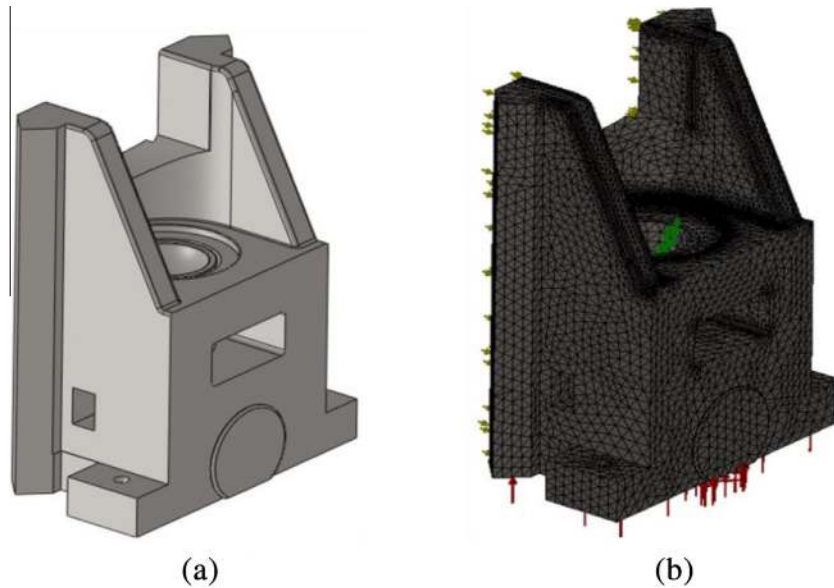
Fig. 9. Ram assembly: (a) 3D CAD model, (b) Meshed model with loads and fixtures.

details. Certain assumptions are made such as the ram assembly is considered as mono block and knob contact surface is fixed. Fig. 9 (b) shows the meshed model of ram group. The mesh is high quality so that the effect of force on each portion of components is not the same. The discretization is performed in order to analyze each small division separately. Since ram and connecting rod are in interaction with each other, the same loading distribution is transmitted to the connecting rod. In this study, an external force, considered as a pressure, of 500 kN is applied on the bottom side of ram surface contact area of 77,600 mm². A fixed reaction surface is considered on the spherical knob bearing.

Fig. 9(b) shows loading and boundary conditions. Green arrows show fixed surfaces, yellow arrows show sliding surfaces, and red arrows show applied pressure on the ram assembly.

The main concern is the total deformation and von-Mises stresses acting on the ram assembly. Fig. 10(a) shows stresses acting on the ram assembly, in which the maximum stresses are indicated by red color. The total deformation of ram assembly is shown in Fig. 10(b). The deformation on ram is not the same everywhere. Fig. 10(c) shows the values for factor of safety. Table 6 also shows results of FEA. The minimum safety of the shaft is about 2 on the ram safety block that is a changeable part. On the other hand, in real case, this value is over 3 for the entire ram assembly.

5.4. Main press body

The assembly of the main body consists of several parts such as right-left sides, bottom sides, top sides, back sides, and bolster (table) in Fig. 11(a). Table 7 shows main body mesh details. The main body is supported by the fins at right and left sides. The main body assembly is considered as mono block and bottom sides are fixed as an assumption. The meshed model of the body assembly is shown in Fig. 11(b) with loading and boundary conditions. In this study, three external forces are considered. They are bolster reaction (6.4 MPa due to 500 kN) as indicated by brown arrows, ram bearing reaction of 30 kN as indicated by purple arrows (surface area: 2 × 96,000 mm²), and crank bearing reaction (13 MPa due to 500 kN) as indicated by red arrows (contact area: 2 × 29,680 mm²). A fixed reaction surface (280,000 mm²) is considered on the bottom side, which is indicated by green arrows. The maximum stresses acting on the main body assembly are seen

Table 6
Ram simulation details.

Ram material: St 52	
Mesh	
Number of nodes: 306,564	Number of elements: 205,263
Global size:14 mm	Tolerances: 0.71
FEA	
von Mises stress: 205.3 MPa	Max. deformation: 0.077 mm

in Fig. 12(a) as indicated by red color. The total deformation of main body assembly is given in Fig. 12(b) where the deformation is not the same everywhere. Fig. 12(c) shows the values of factor of safety. Table 7 also shows results of FEA. The minimum safety of the body is about 2 on the main body although the overall FS value is over 3 in general analysis.

5.5. Pinion-shaft assembly

The assembly of pinion-shaft includes a pinion gear and a shaft, as in Fig. 13(a). The shaft is actuated by servo motor and gear box, and hence only torque is acting on the assembly. There are assumptions that the pinion-shaft assembly is considered as a mono block, and one gear contact surface is fixed. Fig. 13(b) shows the meshed model of assembly. Fig. 13(b) shows loading and boundary conditions. In this study, the external force is considered as a torque of 4000 Nm as indicated by purple arrows (surface area: 55,100 mm²). A fixed reaction surface is considered on the gear with 1960 mm² surface, as indicated by green arrows. Navy blue arrows indicate the bearings with 2 × 46,500 mm². Table 8 shows pinion shaft mesh details.

Fig. 14(a) shows the stresses acting on pinion-shaft assembly. The maximum stresses are shown by red color. The total deformation is also shown in Fig. 14(b), and Fig. 14(c) gives the values of FS. The minimum safety of the shaft is about 1.5 on the assembly, but the overall FS value is over 3 in general analysis.

6. Experimental implementation

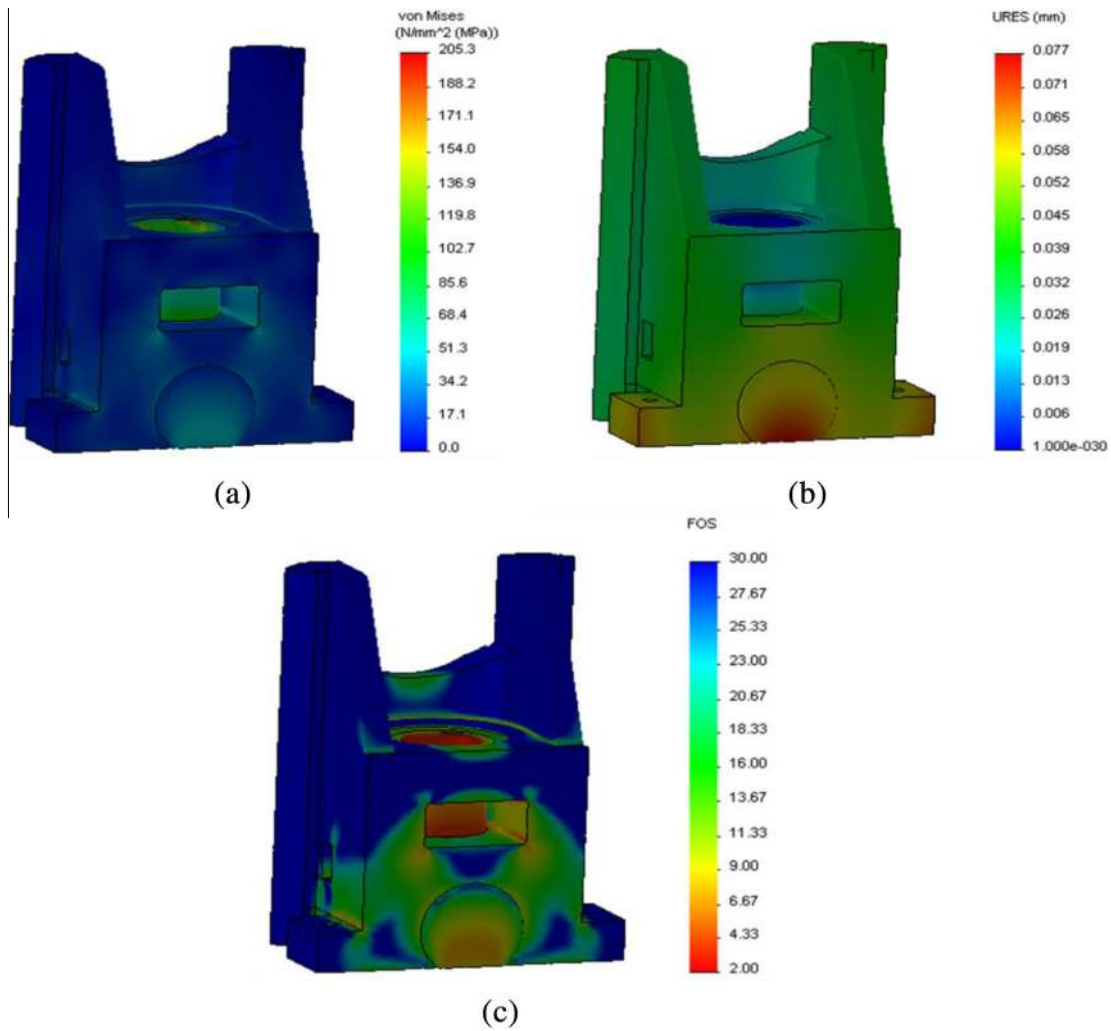Having completed structural design and analysis, servo crank press has been manufactured is shown in Fig. 16. Fig. 15

Fig. 10. Structural analysis results of the ram assembly: (a) von-Mises stress, (b) Deformation, (c) Factor of safety.
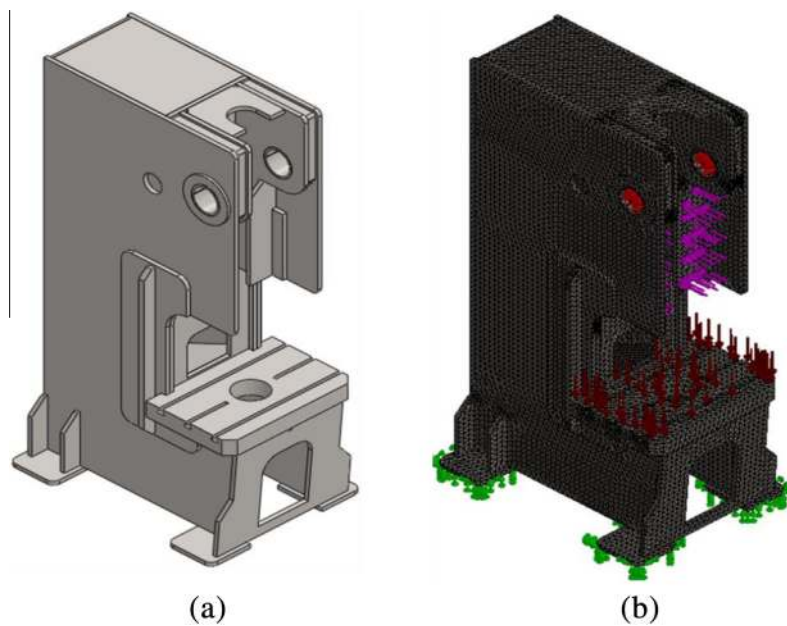

Fig. 11. Main body assembly: (a) 3D CAD model, (b) Meshed model with loads and fixtures.

Table 7

Main body simulation details.

Main body material: St 37	
Mesh	
Number of nodes: 186,401	Number of elements: 103,230
Global size: 30.8 mm	Tolerances: 1.5 mm
FEA	
von Mises stress: 142 MPa	Max. deformation: 0.423 mm

(a) presents mechanic parts before assembly and Fig. 15(b) shows assembly of servo crank press by equipment: servo motor, servo gearbox, sensors and control & automation hardware.

Manufacturing performance of the press is realized loads of 0–500 kN. Different motion scenarios are applied on the servo crank press: *crank motion, dwell motion, link motion,* and *soft motion* without reaction force. They are all performed with 20 spm stroke
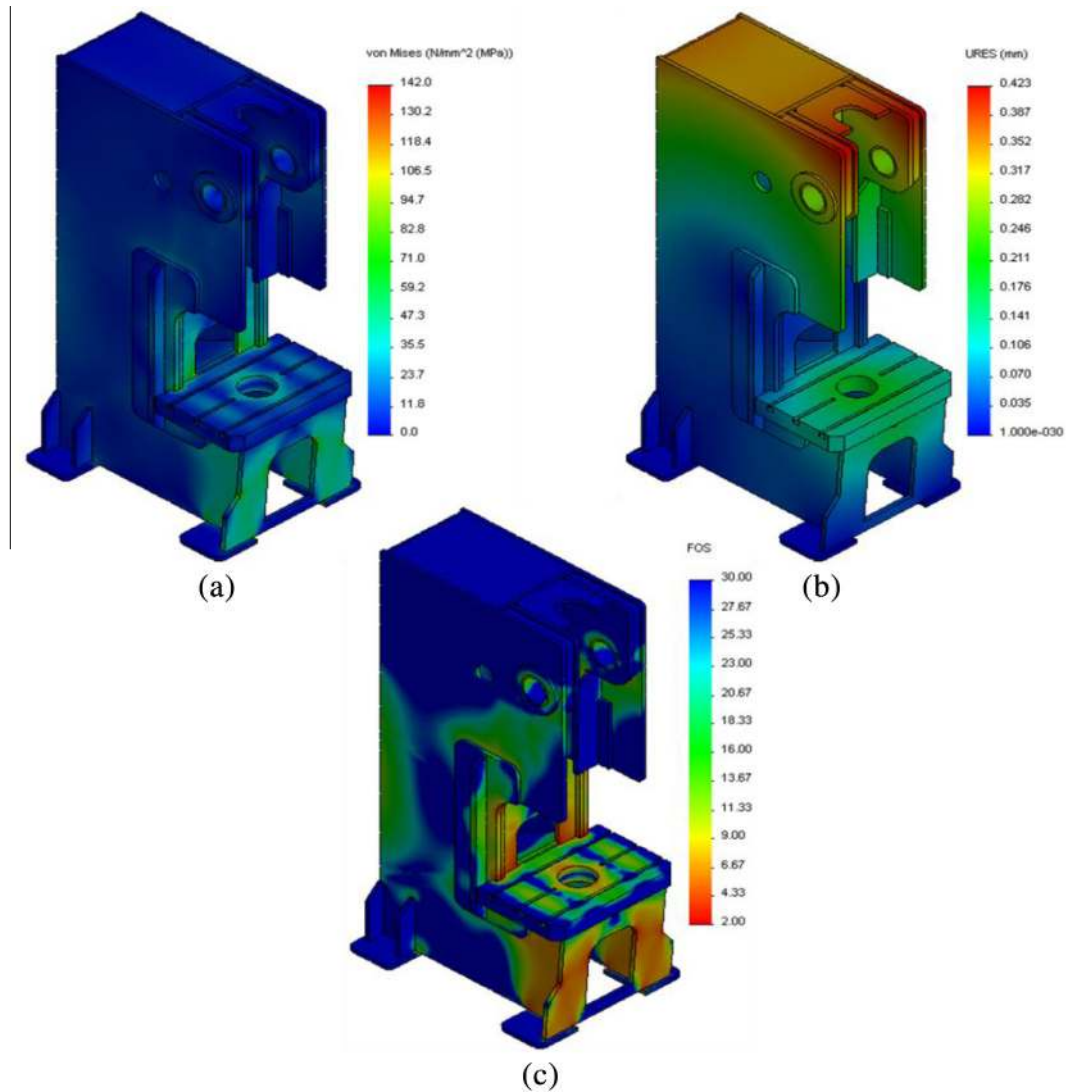

Fig. 12. Structural analysis results of the main body assembly: (a) von-Mises stress, (b) Deformation, (c) Factor of safety.
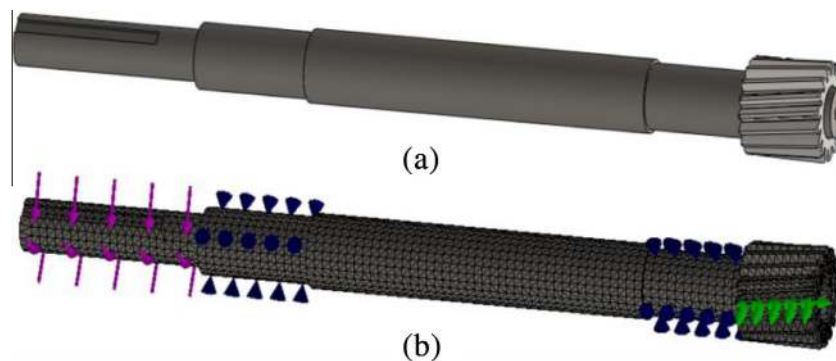

Fig. 13. Pinion shaft assembly: (a) 3D CAD model, (b) Meshed model with loads and fixtures.

Table 8
Pinion shaft simulation details.

Main body shaft material: 42CrMo4	Main body pinion material: 30CrNiMo8
Mesh	
Number of nodes: 56,727	Number of elements: 36,886
Global size: 12.13 mm	Tolerances: 0.6 mm
FEA	
von Mises stress: 772.7 MPa	Max. deformation: 0.428 mm

velocity [26]. Fig. 16(a) shows *command* (with blue straight line) as well as *responses* of the ram motion as "*from motor*" (with red dashed line where data are converted from experimental response of the motor by using kinematic equations) and "*linear encoder*" (shown by green dotted line where data are taken from linear encoder on the ram). A delay time (16 ms) is realized between *command* and *responses*. Experimental and simulated torques for
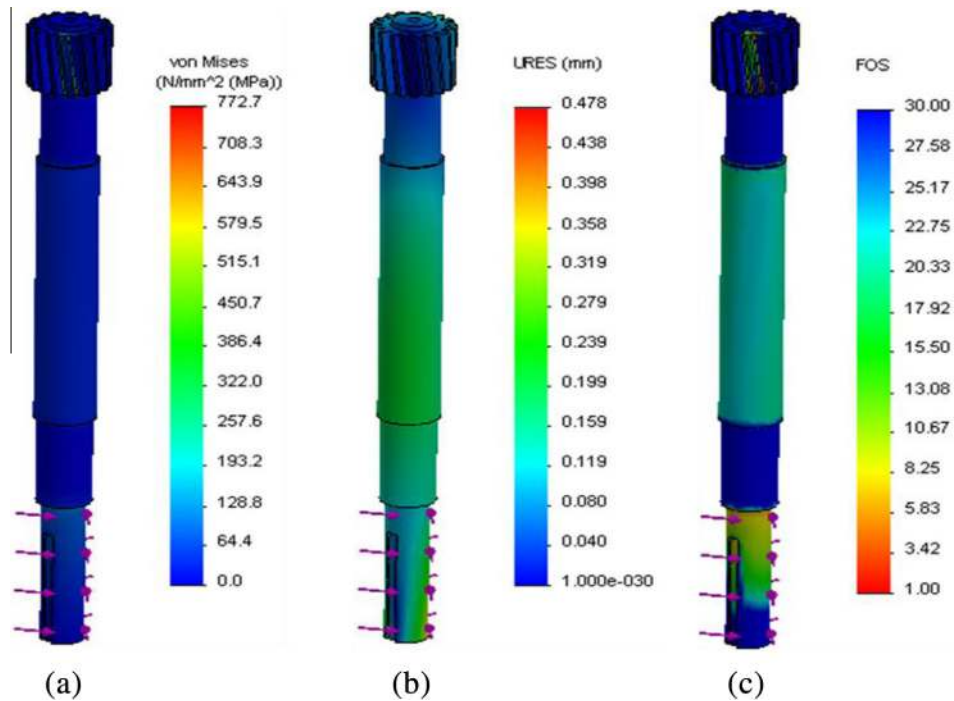

Fig. 14. Structural analysis results of the pinion-shaft assembly: (a) von-Mises stress, (b) Deformation, (c) Factor of safety.
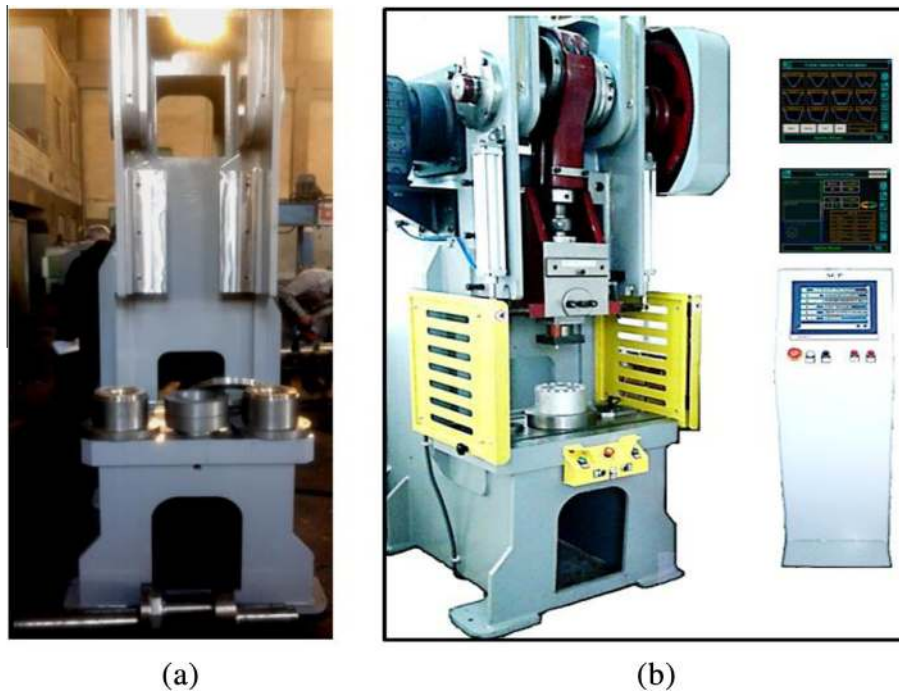

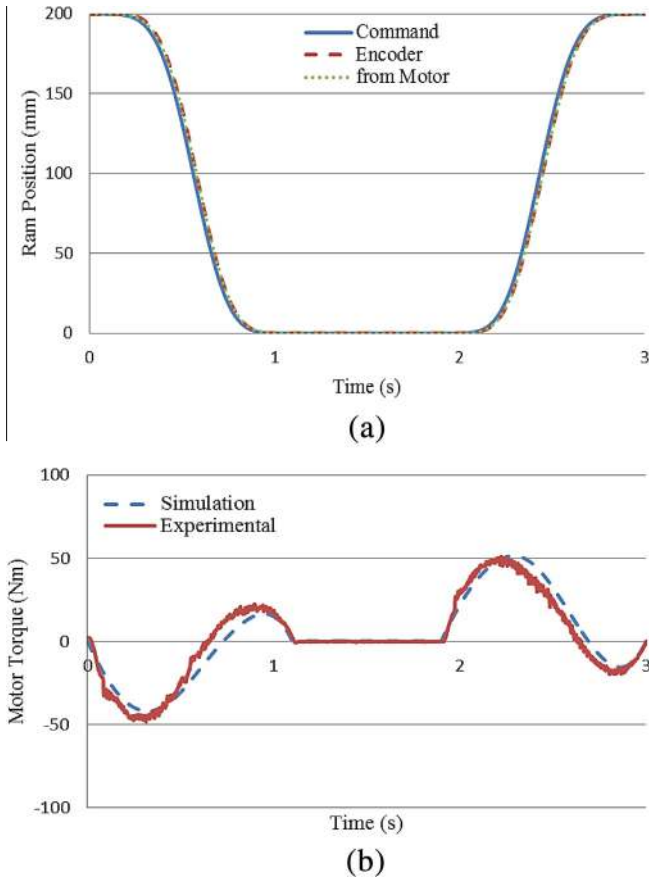**Fig. 15.** Manufactured servo press.

Fig. 16. (a) Ram position command and responses and (b) Motor torque simulation and experimental results.

dwell motion is shown in Fig. 16(b). The results show good agreements.

7. Conclusions

Servo crank press system is constructed in dynamic and static parts. In this study, dynamic parts are crank and helical gear, pinion shaft and helical gear, connecting rod, and ram. Static parts are C-type mono-block body and its welded components. The design was started by selection of sleeve bearings since they are the weakest components on the press system. The design was based on the methods of machine elements in which safety factor was selected as two. This article presents 3D CAD modeling and FEA of the components in servo crank press. A dedicated design approach is employed. CAD designs for all parts are completed by considering dynamic limits. All parts of the servo press are analyzed as structural static during FEA. The results are revealed that the press machine has operated within the required safety limits. Different loads and motion scenarios are successfully tested. Here dwell motion is presented to show system implementation. System torques is also measured.

Acknowledgements

Appendix A

A.1. Bearing design procedures

Step 1

According to dynamics of mechanism, the maximum values for load and angular velocity in the process are found. The shaft diameters for different type of bearings are defined by using these values. A chart is used (Fig. A.1). This chart is based on a life of 10,000 h for rubbing, rolling and porous metal bearings [42].

Step 2

In designing a bushing, it is recommended that length/diameter (L/D) ratio will be in the range of $0.5 \leqslant B/D \leqslant 2$. Using different values, B and D dimensions are determined by Eq. (A.1) [1].

Step 3

V_s is the surrounding velocity of bearing, defined by Eq. (A.1) where W is angular velocity. V_s and PV_s must be under the bearing material's capacity [1,30].

$$V_s = \frac{WD}{2} \tag{A.1}$$

Step 4

Dimensionless relative bearing clearance (Ψ) is given in Eq. (A.2) for bronzes, which can also be obtained by Eq. (A.3). After determining Ψ, the clearance between shaft and bearing (c) can be found from Eq. (A.2) where r and R are the radius of shaft and bearing, respectively [30]. Instead of r (that is unknown), R (that is approximately same as r) can be used in Eq. (A.2). This is necessary for the determination of clearance. Recommended clearance values range from 0.2 to 0.5% of the journal diameter [33]. R can then be determined.

$$\Psi = \frac{\Delta r}{r} = \frac{R - r}{r} = \frac{2c}{D} \tag{A.2}$$

$$\Psi \cong \frac{0.8}{1000} \sqrt[4]{V_s} \tag{A.3}$$

Step 5

Film thicknesses are defined through Eqs. (A.4) and (A.5) as the minimum (h_0) and the maximum (h_{max}). After h_0 is selected based on Trumpler's criteria as given in Eq. (A.4), Eq. (A.5) is given as the eccentricity (e) [1]. This value is used in Eq. (A.6) to define the maximum film thickness (h_{max}). Dimensionless relative eccentricity (ε) is found by using Eq. (A.7), which is usually desired as bigger than 0.5 [1,30].

$$h_0 \geqslant 0.00508 + 0.00004D \tag{A.4}$$

$$h_0 = c - e \tag{A.5}$$

$$h_{max} = c + e \tag{A.6}$$

$$\varepsilon = \frac{e}{c} \tag{A.7}$$

Step 6

Coefficient of friction (f) is necessary for calculation of bed heat. Eq. (A.8) is used for friction [30]. The ratio of f/Ψ is used in the next step.

$$f = \frac{1 + 2\varepsilon^2}{3\varepsilon}\Psi \tag{A.8}$$
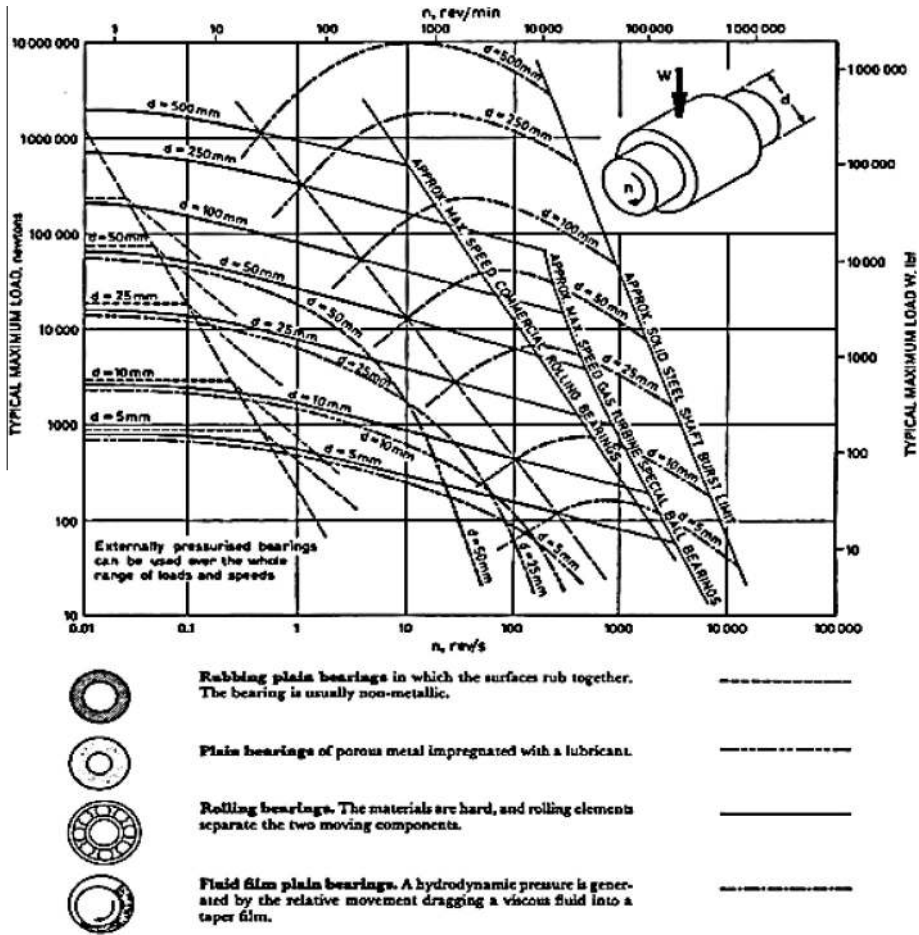
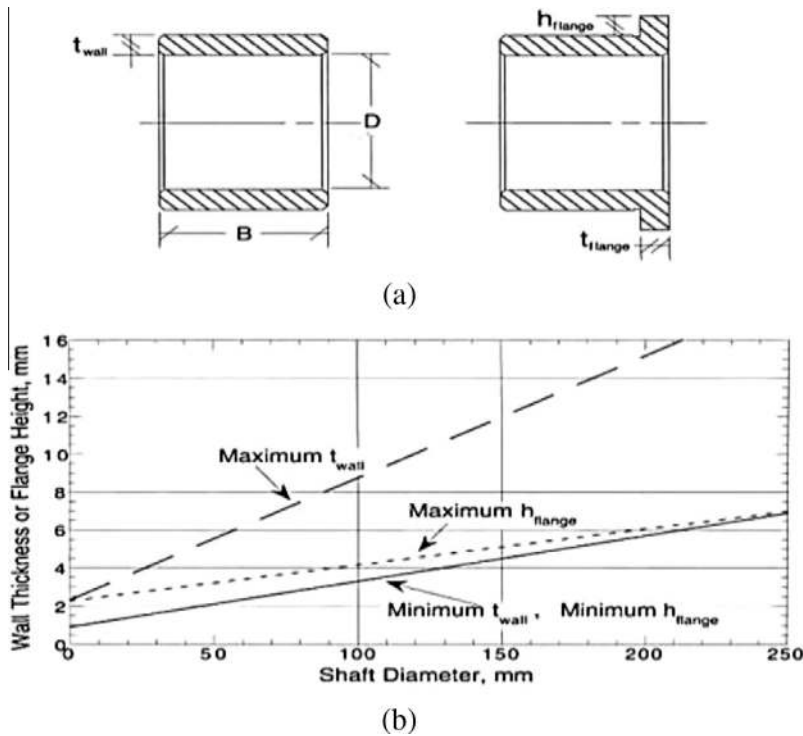Fig. A.1. Bearings capacity selection chart [30,42].

Fig. A.2. (a) Thickness and flange representation of bearing, (b) the maximum and the minimum values of thicknesses and flanges [33].

Table A.1
Determination of flow rate factor (β_Q) based on eccentricity (ε) [30].

ε	0.9	0.8	0.7	0.6	0.5
β_Q (for $B/D = 1$)	8	12	18	25	33
β_Q (for $B/D = 0.5$)	6	14	25	45	–

Step 7

Somerfield number (S), the characteristic number of bearing, is found via Eq. (A.9). Generalized Somerfield number is given in Eq. (A.10) where N is the angular velocity (rev/s), μ is the viscosity of oil film (Pa*s), and P is the bearing pressure (MPa). Somerfield number is very important in lubrication analysis specified by designer [1,30].

$$\frac{f}{\Psi} = 2\pi^2 S \qquad (A.9)$$

$$S = \left(\frac{r}{c}\right)^2 \frac{\mu N}{P} \qquad (A.10)$$

Step 8

Fig. A.2(a) presents bearing thickness and flange size as t_{wall} and h_{flange}, respectively. The overall thickness/diameter ratio is not critical, but the minimum and the maximum wall thicknesses with recommended flange sizes are given in Fig. A.2(b) according to ISO-4379 [33]. The wall thickness is calculated from Eq. (A.11) [43].

$$\text{Light}: t_{wall} = 0.08D + 0.8 \text{ (mm)}$$
$$\text{Medium}: t_{wall} = 0.08D + 1.6 \text{ (mm)} \qquad (A.11)$$
$$\text{Heavy-duty}: t_{wall} = 0.08D + 3.2 \text{ (mm)}$$

Step 9

For hydrodynamic oil film, the lubricant flow rate (Q) is defined by using Eq. (A.12). Here, β_Q is the flow rate factor that depends on ε value, as given in Table A.1 [30].

$$Q = \frac{60 f D^2 B N}{320 \beta} \text{ [lt/min]} \qquad (A.12)$$

References

[1] J. Nisbett, R. Budynas, Shigley's Mechanical Engineering Design, McGraw-Hill, New York, 2008.
[2] E. Koc, Makina Elemanları Cilt-1, Nobel Yayın Evi, Adana, 2004.
[3] J. Song, C.R. Mischke, R.G. Budynas, X. Liu, Z. Gao, Mechanical Engineering Design, McGraw-Hill, New York, 1989.
[4] B.A. Szabo, I. Babuška, Finite Element Analysis, John Wiley & Sons, 1991.
[5] D.G. Lee, J. Do Suh, H. Sung Kim, J. Min Kim, Design and manufacture of composite high speed machine tool structures, Compos. Sci. Technol. 64 (2004) 1523–1530.
[6] J. Suh, D. Lee, Design and manufacture of hybrid polymer concrete bed for high-speed CNC milling machine, Int. J. Mech. Mater. Des. 4 (2008) 113–121.
[7] X. Min, J. Shuyun, C. Ying, An improved thermal model for machine tool bearings, Int. J. Mach. Tools Manuf 47 (2007) 53–62.
[8] R. Neugebauer, C. Scheffler, M. Wabner, M. Schulten, Advanced state space modeling of non-proportional damped machine tool mechanics, CIRP J. Manuf. Sci. Technol. 3 (2010) 8–13.
[9] R. Neugebauer, C. Scheffler, M. Wabner, Implementation of control elements in FEM calculations of machine tools, CIRP J. Manuf. Sci. Technol. 4 (2011) 71–79.
[10] S. Hu, Q. Yang, B. Peng, H. Wang, Direct-drive bi-rotary milling head variable load thermal characteristics analysis, AASRI Procedia 3 (2012) 270–276.
[11] H. Haddad, M. Al Kobaisi, Optimization of the polymer concrete used for manufacturing bases for precision tool machines, Compos. Part B: Eng. 43 (2012) 3061–3068.
[12] R. Patel, S. Dubey, K. Pathak, Analysis of infilled beams using method of initial functions and comparison with FEM, Eng. Sci. Technol., Int. J. 17 (2014) 158–164.
[13] M. Mohammed Asif, K.A. Shrikrishana, P. Sathiya, Finite element modelling and characterization of friction welding on UNS S31803 duplex stainless steel joints, Eng. Sci. Technol., Int. J. 18 (2015) 704–712.
[14] A.C.K. Choi, D.S.K. Chan, A.M.F. Yuen, Application of virtual assembly tools for improving product design, Int. J. Adv. Manuf. Technol. 19 (2002) 377–383.
[15] W.L. Xu, D. Lewis, J.E. Bronlund, M.P. Morgenstern, Mechanism, design and motion control of a linkage chewing device for food evaluation, Mech. Mach. Theory 43 (2008) 376–389.
[16] L.M. Gómez-López, V. Miguel, A. Martínez, J. Coello, A. Calatayud, Simulation and modeling of single point incremental forming processes within a solidworks environment, Procedia Eng. 63 (2013) 632–641.
[17] R.M.d.S. Araugio, J. Landre Jr., D.d.L.A. Silva, W. Pacheco, M.M. Pithon, D.D. Oliveira, Influence of the expansion screw height on the dental effects of the hyrax expander: A study with finite elements, Am. J. Orthod. Dentofac. Orthop. 143 (2013) 221–227.
[18] M. Nakauma, S. Ishihara, T. Funami, T. Yamamoto, M. Higashimori, Deformation behavior of agar gel on a soft substrate during instrumental compression and its computer simulation, Food Hydrocolloids 36 (2014) 301–307.
[19] R. Halicioglu, L.C. Dulger, A.T. Bozdana, Mechanisms, classifications, and applications of servo presses: A review with comparisons, in: Proceedings of the Institution of Mechanical Engineers, Part B: Journal of Engineering Manufacture, 2015. doi: 0954405415600013.
[20] E. Doege, M. Hindersmann, Optimized kinematics of mechanical presses with noncircular gears, CIRP Ann. – Manuf. Technol. 46 (1997) 213–216.
[21] S. Spiewak, R. Duggirala, K. Barnett, Predictive monitoring and control of the cold extrusion process, CIRP Ann. – Manuf. Technol. 49 (2000) 383–386.
[22] K.-H. Chang, S.-H. Joo, Design parameterization and tool integration for CAD-based mechanism optimization, Adv. Eng. Softw. 37 (2006) 779–796.
[23] M.N. Abdullah, V.V. Telegin, Modeling of dynamic processes of the main executive mechanism of the hot-crank press, Al-Rafadain Eng. J. 19 (2011) 1–10.
[24] E. Zheng, X. Zhou, Modeling and simulation of flexible slider-crank mechanism with clearance for a closed high speed press system, Mech. Mach. Theory 74 (2014) 10–30.
[25] M.E. Kütük, L.C. Dülger, A hybrid press system: Motion design and inverse kinematics issues, Eng. Sci. Technol., Int. J. 19 (2016) 846–856.
[26] R. Halicioglu, Design, Synthesis and Control of a Mechanical Servo Press: An Industrial Application (Ph.D. thesis), Mechanical Engineering, University of Gaziantep, 2015.
[27] Coskunoz, Coskunoz metal form, 1 January, 2014, available in http://www.macos.com.tr/.
[28] R. Halicioglu, L. Dulger, A. Bozdana, Modelling and simulation based on matlab/simulink: a press mechanism, in: Journal of Physics: Conference Series, IOP Publishing, 2014. pp. 012053.
[29] R. Halicioglu, L. Dulger, A. Bozdana, Servo pres tasarımı ve dinamik modeli: uygulamalı bir örnek, in: TRISTOMM-UMTS 2015, İzmir, 2015, pp. 963–970.
[30] E. Koc, Makina Elemanları Cilt-2, Nobel Yayın Evi, Adana, 2004.
[31] W. Glaeser, Handbook: Design of Boundary Lubricated Cast Bronze Bearings, Cast Bronze Bearing Institute Inc., 1978.
[32] W. Glaeser, Materials for Tribology, Elsevier, 1992.
[33] Copper Development Association Inc., Cast Copper Alloy Sleeve Bearings Selection Guidewith Bound and Hydro Computer-assisted Sleeve Bearing Design, 260 Madison Avenue, New York, 1997.
[34] F. Song, Y. Ni, Z. Tan, Optimization design, modeling and dynamic analysis for composite wind turbine blade, Procedia Eng. 16 (2011) 369–375.
[35] RBC, Spherical plane bearings: RBC catalog, 01 January, 2015, available in http://rbcbearings.com/literature/pdfs/SPB052010.pdf.
[36] K. Im, R.L. Shaw, J.-H. Lee, K.-K. Kim, K.-O. Nam, S.-H. Jung, H.-S. Hwang, H.-K. Park, The design of the assembly tools for the ITER tokamak, Fusion Eng. Des. 86 (2011) 659–662.
[37] Rolex Metal Distributors. Mechanical Properties, Mumbai-India.
[38] D.G. Ullman, The Mechanical Design Process, McGraw-Hill, 2002.
[39] U. Jindal, Machine Design, Pearson Education, India, 2010.
[40] H. Filiz, Machine Tool Design: Lecture Notes, Gaziantep University, Gaziantep, 2011.
[41] SolidWorks, 01 January, 2012, available in www.solidworks.com.
[42] M.J. Neale, Tribology Handbook, Butterworth-Heinemann, 1995.
[43] S.J. Hudak, Bearing Design Guide, Atlas Bronze, 1995.